Wave orbital velocity skewness and linear transition ripple migration: Comparison with weakly nonlinear theory

Anna M. Crawford[1] and Alex E. Hay

Department of Oceanography, Dalhousie University, Halifax, Nova Scotia, Canada

Received 11 December 2001; revised 6 June 2002; accepted 19 December 2002; published 20 March 2003.

[1] Field observations of linear transition ripples during an autumn storm exhibit high correlation between cross-shore ripple migration rate and the skewness of the near-bed wave orbital velocity. For a bimodal spectrum of mixed sea and swell, negatively skewed near-bed orbital velocities were accompanied by offshore ripple migration, while for unimodal swell, ripples migrated onshore under positively skewed velocities. Bispectral analysis and weakly nonlinear wave theory are used to show that the positive and negative velocity skewness arose from higher-order interactions between frequency components of the incident wave spectrum. There is good quantitative agreement between predicted and observed velocity skewness, indicating a connection between ripple migration and wave-wave interactions. *INDEX TERMS:* 4546 Oceanography: Physical: Nearshore processes; 4558 Oceanography: Physical: Sediment transport; 3020 Marine Geology and Geophysics: Littoral processes; 3022 Marine Geology and Geophysics: Marine sediments—processes and transport; 4219 Oceanography: General: Continental shelf processes; *KEYWORDS:* bed form migration, wave nonlinearity, bispectra, nearshore processes

Citation: Crawford, A. M., and A. E. Hay, Wave orbital velocity skewness and linear transition ripple migration: Comparison with weakly nonlinear theory, *J. Geophys. Res.*, *108*(C3), 3091, doi:10.1029/2001JC001254, 2003.

1. Introduction

[2] Although bed form migration is unquestionably the result of sediment transport processes, the complexity of the dynamics involved has yet to be incorporated into a comprehensive theory. Nevertheless, it is frequently supposed that ripple migration rate is related to net transport, particularly the bed load component, and further that net bed load transport rate, while not well understood, is controlled at least in part by higher-order moments of the nearbed velocity [*Bagnold*, 1963; *Fredsøe and Deigaard*, 1992; *Nielsen*, 1992].

[3] The theoretical and observational background for the application of weakly nonlinear theory to nearshore waves is well established [*Elgar and Guza*, 1985a, 1985b]. Observations of higher-order moments such as wave skewness, in the form of bispectra, have been well described by the theory put forward in the early work of *Hasselmann* [1962], *Herbers et al.* [1994], and *Herbers and Burton* [1997]. This theory is suitable for comparison with observations of weakly nonlinear waves at a fixed depth. Shoaling behavior, characterized by evolution of wave skewness and asymmetry, is better modeled using a treatment that includes depth change dependence, such as Boussinesq theory [*Elgar and Guza*, 1985b; *Norheim et al.*, 1998].

[4] The purpose of this paper, continuing from earlier work presented by *Crawford and Hay* [2001], is to examine observed near-bed velocity skewness in relation to cross-shore ripple migration by comparing the velocity bispectra with theoretical bispectra derived following the work of *Hasselman et al.* [1963] and *Herbers et al.* [1992]. This comparison will unambiguously determine the physical origins of the positive and negative velocity skewness and thereby identify a mechanism leading to onshore and offshore ripple migration.

[5] There are few reported field measurements of ripple migration in the literature, and fewer relating observed migration to local wave forcing. In 1988, *Boyd et al.* [1988] commented that at that time, those of *Dingler* [1974] were the only published field observations other than their own. Subsequently, additional observations have been reported, for example, by *Vincent and Osborne* [1993], *Hay and Bowen* [1993], *Amos et al.* [1999], and *Traykovski et al.* [1999]. *Boyd et al.* [1988] and *Vincent and Osborne* [1993] attempted to relate ripple migration velocity to various nondimensional parameters and characteristic flow velocities; these efforts were largely inconclusive. *Amos et al.* [1999] observed ripples in a combined flow situation with a strong current component and found that the ripple migration velocity was related more closely to the current flow, with the wave component enhancing sediment mobility. *Traykovski et al.* [1999] found qualitative agreement between the cumulative integrals of $\overline{u^3}$ and shoreward ripple displacement in wave-dominated flow on the continental shelf.

[6] *Crawford and Hay* [2001] presented observations of the migration of linear transition ripples in the outer surf zone on a sandy pocket beach. Linear transition ripples are low relief, short wavelength bed forms occurring at high wave energies, just below the flatbed transition [*Conley and*

[1] Now at Mine and Torpedo Defence, Defence R&D Canada–Atlantic, Dartmouth, Nova Scotia, Canada.

0148-0227/03/2001JC001254$09.00

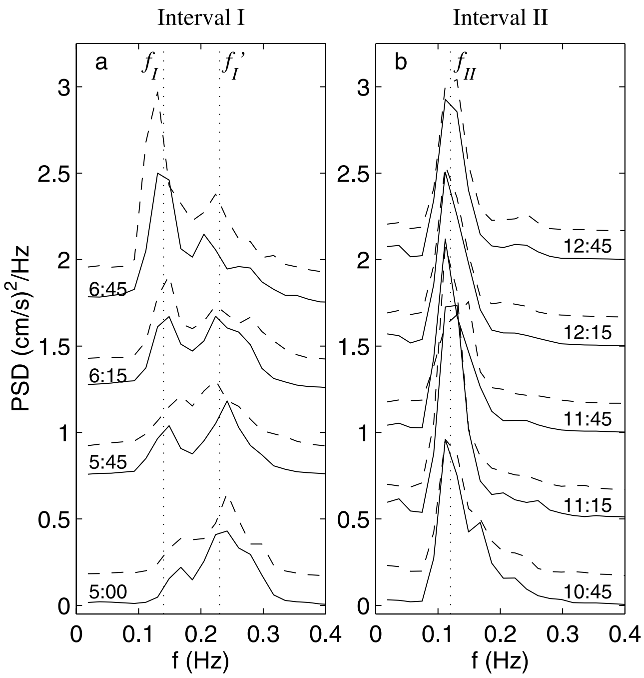

Figure 1. Power spectral densities of CDP-measured near-bed orbital velocity during (a) interval I and (b) interval II. The spectra pairs (alternating solid and dashed lines) are from 7.2-min CDP runs 10 min apart, labeled with the start time of the first run, with a *y*-axis offset proportional to the time elapsed from the first CDP run in each interval. Ensemble-averaged peak frequencies are indicated by dotted lines.

Inman, 1992; *Dingler and Inman*, 1977]. In our previous paper the migration velocity of these bed forms was found to be well correlated with the evolving skewness of the near-bed orbital velocity during a storm event, offshore migration occurring during the growth phase of the storm and onshore migration occurring during the decay phase.

[7] Following a very brief overview of the observations, we will present a comparison of velocity bispectra with theoretical bispectra, including a summary of the derivation of the theoretical bispectrum.

2. Observations

[8] The experiment site was located on Queensland Beach, a pocket beach at the head of St. Margarets Bay, west of Halifax, Nova Scotia, Canada. The suite of instruments deployed included a coherent Doppler profiler (CDP) [*Zedel and Hay*, 1999] for measurement of near-bed velocity, narrow- and wide-beam scanning sonars (A. E. Hay et al., manuscript in preparation; 2003), and a laser-video system [*Crawford and Hay*, 1998] for bed form measurements. The instruments were deployed approximately 60 m from the mean water line in 3.2-m mean water depth. A more complete description of the field site and instrumentation is given by *Crawford and Hay* [2001].

[9] Observations were obtained over an 18-hour period spanning an autumn storm event (year day 261, 1995). During the growth of the storm, as significant wave height increased to a maximum of 1 m, the peak wave period shifted from 4-s sea waves to lower-frequency (7-s) swell. As the storm subsided, the dominant wave energy was at the swell frequency. Of interest were two time periods before and after the peak of the storm when linear transition ripples were present, designated intervals I and II. During both intervals, the grain roughness Shields parameter was between 0.3 and 0.6, increasing through interval I and decreasing through interval II (the median grain diameter was 174 μm). The evolution of the orbital velocity power spectrum through the two intervals is shown in Figure 1. The ensemble average peak frequencies were $f_{\mathrm{I}} = 0.14$ Hz and $f_{\mathrm{I}}' = 0.23$ Hz during interval I and $f_{\mathrm{II}} = 0.12$ Hz during interval II. The subscripts denote the interval, with the primed variable referring to the sea frequency in interval I and the unprimed variable referring to the swell.

[10] The response of the linear transition ripples to the changing wave forcing during these two time periods was in the measured ripple migration velocities. There was very little change in bed form geometry: The average ripple wavelength was 8.5 cm for both intervals, with a steepness (height/wavelength) of 0.04 measured during interval I. Bed form profiles were obtained using a fixed narrow-beam sonar during both intervals, and higher resolution measurements were obtained during interval I using the laser-illuminated video imaging system [*Crawford and Hay*, 1998]. Ripple displacement (and hence migration velocity) was determined from the spatial lag of the peak correlation between successive averaged bed profiles. The migration velocities were found to be well correlated with the skewness of the demeaned near-bed orbital velocity, as shown in Figure 2. Note that this figure differs slightly from that

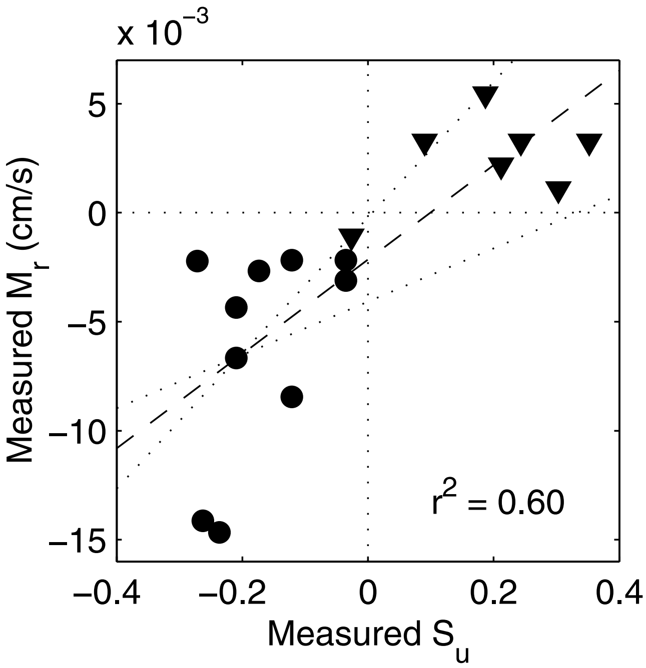

Figure 2. Transition ripple migration velocity M_r plotted against orbital velocity skewness S_u. The dashed and dotted lines are a least squares linear regression and the 95% confidence interval. Circles denote measurements during interval I (both acoustic and laser-video measurements) and triangles denote interval II (acoustic measurements).

presented by *Crawford and Hay* [2001]. The laser-video migration velocity data have been reprocessed so that the laser-video time segments coincide exactly with the 7.2-min CDP runs. The correlation is slightly lower due to the two points in the lower left, but overall the relationship between migration rate and velocity skewness is still clear. In particular, offshore ripple migration is associated with negative skewness and onshore migration is associated with positive skewness.

3. Velocity Bispectra

[11] The bispectrum has been shown to be a valuable tool for investigating nonlinearities in shoaling waves [*Hasselman et al.*, 1963; *Elgar and Guza*, 1985a; *Herbers et al.*, 1992]. The complex digital bispectrum B of a stationary, Gaussian time series is calculated from

$$B(f_1,f_2) = E[C(f_1)C(f_2)C(-f_1-f_2)], \tag{1}$$

where $E[\quad]$ denotes the expectation value and $C(f)$ is the complex Fourier coefficient with frequency $f(-f_N \leq f \leq f_N$, where f_N is the Nyquist frequency). From symmetry considerations, the bispectrum is unique in a frequency-frequency domain bounded by $0 \leq f_1 \leq f_2$ and $f_1 + f_2 \leq f_N$. A property of the bispectrum that is particularly useful when applied to a shoaling wave time series is that the third moment can be obtained from the real part [*Elgar and Guza*, 1985a]. Taking account of the symmetry in frequency-frequency space, this is written as

$$E\left[u(t)^3\right] = 12\sum_{i,j,i>j}\Re\left\{B\left(f_i,f_j\right)\right\} + 6\sum_j\Re\left\{B\left(f_j,f_j\right)\right\}, \tag{2}$$

where $\Re\{\quad\}$ denotes the real part. The third moment $E[u^3]$ and skewness S are related by

$$S = \frac{E\left[u(t)^3\right]}{E\left[u(t)^2\right]^{3/2}} = \frac{\overline{u^3}}{u_{\mathrm{rms}}^3}, \tag{3}$$

where the expectation and average (denoted by the over bar) values are assumed to be equivalent. Examining the real part of the bispectrum in frequency-frequency space reveals the interactions at pairs of frequencies that contribute to the total skewness.

[12] The real part of the observed bispectral density ($\Re\{B(f_1, f_2)\}/\Delta f^2$ where Δf is the frequency resolution) during the two time intervals is shown below the diagonals in Figure 3. The 7.2-min CDP velocity records were resampled from 28 to 9.6 Hz (12,000 to 4096 samples). This was done for comparison of the skewness of the measured velocity with that of velocity calculated using linear theory from surface elevation sampled at 8 Hz. This comparison was favorable, indicating a suitably low level of wave nonlinearity [*Crawford and Hay*, 2001]. Bispectra were then calculated from 512-sample segments (Hanning windowed) with 75% overlap and ensemble averaged, then smoothed by two-point merging in both frequency directions. All the CDP runs occurring during each time period (see Figure 1) were included in the calculations: eight runs during interval I and 10 during interval II, giving 252 and 316 degrees of freedom, respectively.

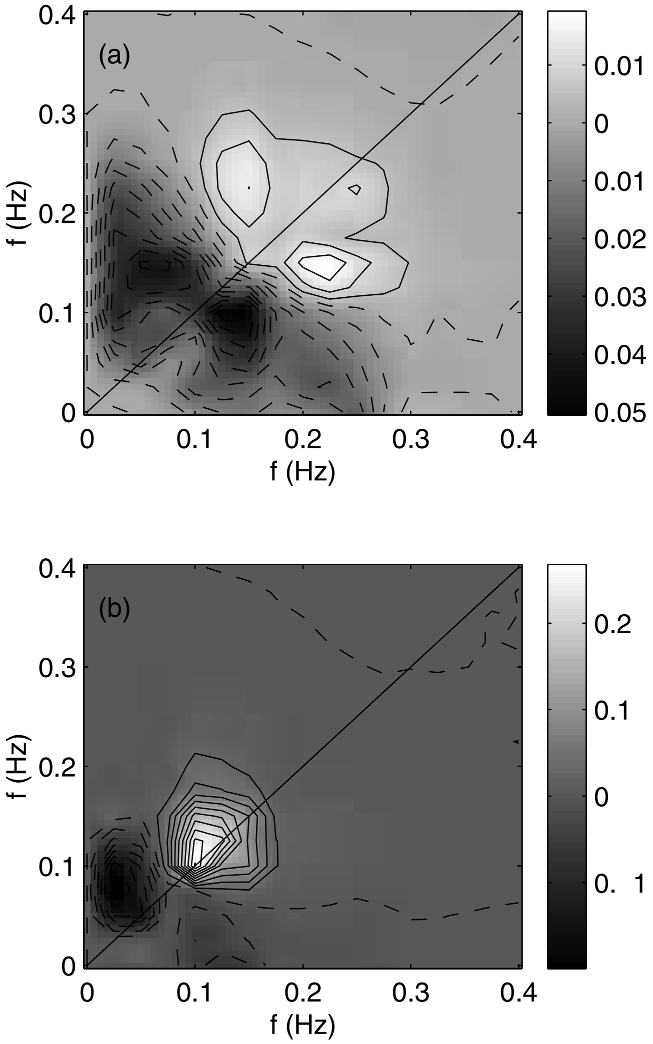

Figure 3. The real part of the observed bispectral density (below the diagonal) and the theoretical bispectral density (above the diagonal) during (a) interval I and (b) interval II. Dashed contours are negative values and solid are zero and positive, at intervals of 0.002 in Figure 3a and 0.005 in Figure 3b. Shaded scales are shown by the bars on the right.

[13] An expression for the theoretical bispectrum can be derived as follows [*Hasselman et al.*, 1963]: The Fourier components of the time series can be considered as perturbation expansions,

$$C(f) = C^{(1)}(f) + C^{(2)}(f) + \ldots, \tag{4}$$

and the second-order contributions can be expressed as functions of the first order terms:

$$C^{(2)}(f) = \sum_{f_1+f_2=f} K(f_1,f_2)C^{(1)}\cdot(f_1)C^{(1)}(f_2), \tag{5}$$

where $K(f_1, f_2)$ is a coupling coefficient between $C^{(1)}(f_1)$ and $C^{(1)}(f_2)$. To lowest (third and fourth) orders, the bispectrum can then be written (by substituting equation (4) into equation (1)) as

$$\begin{aligned} B(f_1,f_2) = {} & E\left[C^{(1)}(f_1)C^{(1)}(f_2)C^{(1)}(-f_1-f_2)\right] \\ & + E\left[C^{(1)}(f_1)C^{(1)}(f_2)C^{(2)}(-f_1-f_2)\right] \\ & + E\left[C^{(1)}(f_1)C^{(2)}(f_2)C^{(1)}(-f_1-f_2)\right] \\ & + E\left[C^{(2)}(f_1)C^{(1)}(f_2)C^{(1)}(-f_1-f_2)\right], \end{aligned} \tag{6}$$

where the first triple-product term vanishes for a Gaussian process. If the spectrum $F(f)$ is written

$$F(f) = E\left[C^{(1)}(f)C^{(1)}(-f)\right], \tag{7}$$

then, using equation (5)

$$\begin{aligned} B_t(f_1,f_2) = 2\,[& F_{(f1)}F_{(f2)}K(-f_1,-f_2) \\ & + F(f_1)F(f_1+f_2)K(-f_1,f_1+f_2) \\ & + F(f_2)F(f_1+f_2)K(-f_2,f_1+f_2)], \end{aligned} \tag{8}$$

where the notation B_t has been used to distinguish this theoretical expression from the observed bispectrum (equation (1)). The coupling coefficient $K(f_1, f_2)$ between the horizontal velocity spectra components can be derived from that for the velocity potential given by *Hasselman et al.* [1963]. For the simplified case of parallel, shore-normal wave vectors obeying the dispersion relation

$$\omega^2 = gk \tanh kh, \tag{9}$$

where $\omega = 2\pi f$ is wave radian frequency, g is gravitational acceleration, h is water depth, and k is wave number, it can be shown that

$$K(f_1,f_2) = G(k_1,f_1,k_2,f_2)\frac{k_1+k_2}{k_1k_2}\frac{\cosh k_1h\cosh k_2h\cosh(k_1+k_2)z}{\cosh k_1z\cosh k_2z\cosh(k_1+k_2)h}. \tag{10}$$

Here z is height above bottom,

$$\begin{aligned} G(k_1,f_1,k_2,f_2) = {} & \frac{1}{2\pi\left(f_+^2-(f_1+f_2)^2\right)} \\ & \cdot\Bigg[(f_1+f_2)k_1k_2[\tanh k_1h\tanh k_2h-1]. \\ & -\frac{1}{2}\left(\frac{f_1k_2^2}{\cosh^2 k_2h}+\frac{f_2k_1^2}{\cosh^2 k_1h}\right)\Bigg] \end{aligned} \tag{11}$$

and

$$(2\pi f_+)^2 = g(k_1+k_2)\tanh(k_1+k_2)h. \tag{12}$$

Equation (8) gives a bispectrum calculated from the velocity spectrum $F(f)$ which only has a real part and does not exhibit the twelvefold symmetry shown by that calculated from the complex Fourier coefficients. This must be taken into consideration when comparing with the observed bispectrum. According to this treatment, the imaginary part of the theoretical bispectrum vanishes [*Hasselman et al.*, 1963; *Herbers et al.*, 1994]. The observed bispectra do have nonzero imaginary content with significant bicoherence, particularly during interval II where evidence of shoaling behavior can be seen in biphases approaching $-45°$. This compares well with observations of shoaling gravity waves reported by *Elgar and Guza* [1985a, Figure 4], showing biphases scattered around $-50°$ at similar water depth and frequencies.

Table 1. Comparison of Summed Calculated and Theoretical Velocity Bispectra With the Third Moment of the Velocity Time Series[a]

Interval	$\langle\overline{u^3}\rangle$	$\Sigma\Re\{B\}$	ΣB_t
I	−0.0033	−0.0036	−0.0042
II	0.0025	0.0026	0.0027

[a]The ensemble average of the third moments of the velocity time series is denoted by $\langle\overline{u^3}\rangle$, $\Sigma\Re\{B\}$ and ΣB_t are the frequency-frequency sums of the real part of the observed bispectra (equation (1)) and the theoretical bispectra (equation (8)).

[14] The theoretical bispectral densities for both time intervals are shown in Figure 3 above the diagonals. These were smoothed by two-point merging in both frequency directions to match the frequency resolution of the observed bispectra, and so are coarser than the spectra shown in Figure 1 by a factor of 2.

[15] Table 1 shows a comparison of values calculated from the velocity time series and from the observed and theoretical bispectra. The bispectra summations were carried out up to 0.4 Hz (over the regions shown in Figure 3); there was no significant contribution to either total above this frequency. The good agreement between the third moment of the time series and the sum of the real part of the observed bispectrum verifies that the bispectrum has been calculated correctly. The favorable comparison between the integral observed values and the sum of the theoretical bispectrum provides quantitative support for the idea that the observed differences in skewness between intervals I and II are due to weakly nonlinear interactions among the frequency constituents of the wave spectrum.

[16] The theoretical bispectral densities compare favorably with the observations (Figure 3). The bispectral peak locations match with spectral peak frequencies to within the lower frequency resolution. Both the observed and theoretical bispectra in interval I exhibit a negative peak at the difference frequency $f_I - f_I'$, though there is more negative (difference) content at lower frequencies in the theoretical bispectrum, probably due to the finite length of the velocity time series from which the observed bispectrum was calculated. The magnitudes of the bispectral peaks in interval I are also well predicted, though the sum of the theoretical bispectrum over-predicts the magnitude of the (negative) third moment. As described in the previous paper [*Crawford and Hay*, 2001], the near-bed velocity skewness was negative throughout interval I, despite the growth of the swell. Observed and theoretical bispectra computed over shorter segments through interval I (disregarding the reduction in statistical significance) show persistence of the negative skewness contribution by the difference interaction between

the sea and swell waves, despite the difference in the wave spectra from beginning to end of the interval (Figure 1). During interval II the strong positive self-self interaction peak is well reproduced in the theoretical bispectrum, however the theoretical bispectrum over-predicts the magnitudes of both the dominant positive peak and the lesser negative peak. Nevertheless, the sum of the theoretical bispectrum during interval II agrees quite well with the third moment of the time series. Over-prediction of the magnitude of bispectral peaks has been noted in similar calculations by other investigators in situations where the Ursell number approaches a significant fraction of 1 (0.6 in a case shown by *Herbers and Burton* [1997]). Here the Ursell number (a/k^2h^3, the ratio of the second-order Stokes expansion coefficient to the first) is smaller: approximately 0.1 in interval I and 0.3 in interval II; the equivalent Ursell number for the difference frequency response in interval I was as large as 0.4.

4. Conclusions

[17] We have shown that the observed velocity skewness is consistent with values predicted using weakly nonlinear wave theory and the full wave energy spectrum. Previously, using a discrete frequency representation of the wave field [*Biésel*, 1952; *Miche*, 1944], we showed that good agreement between predicted and observed skewness could be obtained; however, this approach involves a degree of subjectivity in the choice of representative wave height. Good agreement was obtained using the significant wave height; better was attained with twice the significant wave height [*Crawford and Hay*, 2001]. The full spectrum approach does not suffer from this limitation.

[18] The favorable comparison between observed and predicted velocity skewness reported here clearly indicates that the sign of the skewness derives from wave-wave interactions. This in itself is not a new result. However, the close association between skewness and cross-shore bed form migration (both onshore and offshore) is new. This result provides compelling evidence for a direct connection between nonlinear wave forcing and the cross-shore direction of sediment transport, particularly the bed load component. Thus simplified representations of the incident wave field, such as the commonly used significant wave height and peak period, would predict transport in a direction entirely opposite to that observed when the wave spectrum was bimodal. Therefore it would appear to be essential, when predicting cross-shore sediment transport in the field, that the full wave spectrum be considered for even weakly nonlinear irregular waves. This differs from the provisional conclusion drawn a decade ago by *Kraus and Horikawa* [1990, p. 797], based on the evidence available at the time, that "cross-shore transport produced by irregular waves can be described by simple modification of expressions developed in studies performed using regular waves, if the appropriate statistical wave height parameter is used." In contrast, the present results indicate that the direction of cross-shore bed load transport can change by 180 degrees due solely to differences in the shape of the wave spectrum. Specifically, we have shown, for very similar wave energies and peak periods, that reversals in the direction of cross-shore ripple migration are associated with changes in sign of the near-bed velocity skewness arising from nonlinear interactions among the frequency components of the wave spectrum. Assuming that bed load transport and skewness are related, an assumption consistent with existing bed load transport models, it then follows that the direction of cross-shore bed load transport can also change by 180 degrees, due solely to differences in the wave spectrum shape.

[19] We have demonstrated a clear connection between sum and difference interactions across the frequency spectrum of the incident wave field and onshore/offshore bed form migration. This result has implications for cross-shore sediment transport (bed load) prediction. Sediment transport theories are commonly based on skewness (velocity cubed) [*Bowen*, 1980; *Bailard and Inman* 1981] or on stress [*Sleath*, 1995]: The linkage between observations like those presented here and predictions of sediment transport by these types of theories needs to be explored further.

Notation

x_{rms}	root-mean-square value of x.
$\langle x \rangle$	ensemble average of x.
$\bar{x}$	time average of x.
B	bispectrum.
C	complex Fourier coefficient.
$E[\ ]$	expectation value.
f	frequency.
F	spectrum.
g	acceleration due to gravity.
h	water depth.
k	wave number.
K	coupling coefficient.
M_r	ripple migration velocity.
r^2	correlation coefficient.
$\Re\{\ \}$	real part.
S	skewness.
t	time.
T	spectra peak period.
u	horizontal velocity (demeaned).
z	distance above bottom.
ϕ	velocity potential.
ω	radian frequency.

[20] **Acknowledgments.** This work was funded by the Natural Science and Engineering Research Council of Canada and the U.S. Office of Naval Research Coastal Sciences Program. The authors acknowledge R. T. Guza's comments on previous work, which led to this work.

References

Amos, C. L., A. J. Bowen, D. A. Huntley, J. T. Judge, and M. Z. Li, Ripple migration and sand transport under quasi-orthogonal combined flows in the Scotian Shelf, *J. Coastal Res.*, *15*, 1–14, 1999.

Bagnold, R. A., Beach and nearshore processes, in *The Sea*, vol. 3, edited by M. N. Hill, pp. 507–553, Wiley-Interscience, New York, 1963.

Bailard, J. A., and D. L. Inman, An energetics bedload model for a plane sloping beach: Local transport, *J. Geophys. Res.*, *86*, 2035–2043, 1981.

Biésel, F., Équations générals au second ordre de la houle irrégulaire, *Houille Blanche*, *3*, 372–376, 1952.

Bowen, A. J., Simple models of nearshore sedimentation; beach profiles and longshore bars, in *The Coastline of Canada*, edited by S. B. McCann, pp. 1–11, Geol. Surv. of Canada, Ottawa, Ont., 1980.

Boyd, R., D. L. Forbes, and D. E. Heffler, Time-sequence observations of wave-formed sand ripples on an ocean shoreface, *Sedimentology*, *35*, 449–464, 1988.

Conley, D. C., and D. L. Inman, Field observations of the fluid-granular boundary layer under near-breaking waves, *J. Geophys. Res.*, *97*, 9631–9643, 1992.

Crawford, A. M., and A. E. Hay, A simple system for laser-illuminated video imaging of sediment suspension and bed topography, *IEEE J. Oceanic Eng.*, *23*, 12–19, 1998.
Crawford, A. M., and A. E. Hay, Linear transition ripple migration and wave orbital velocity skewness: Observations, *J. Geophys. Res.*, *106*, 14,113–14,128, 2001.
Dingler, J. R., Wave formed ripples in nearshore sands, Ph.D. thesis, Univ. of Calif., San Diego, 1974.
Dingler, J. R., and D. L. Inman, Wave-formed ripples in nearshore sands, in *Proceedings of the 15th Coastal Engineering Conference*, vol. 2, pp. 2109–2126, Am. Soc. of Civ. Eng., New York, 1977.
Elgar, S., and R. T. Guza, Observations of bispectra of shoaling surface gravity waves, *J. Fluid Mech.*, *161*, 425–448, 1985a.
Elgar, S., and R. T. Guza, Shoaling gravity waves: Comparisons between field observations, linear theory, and a nonlinear model, *J. Fluid Mech.*, *158*, 47–70, 1985b.
Fredsøe, J., and R. Deigaard, *Mechanics of Coastal Sediment Transport*, *Adv. Seri. on Ocean Eng.*, vol. 3, World Sci., River Edge, N. J., 1992.
Hasselmann, K., On the non-linear energy transfer in a gravity-wave spectrum, part 1, General theory, *J. Fluid Mech.*, *12*, 481–500, 1962.
Hasselman, K., W. Munk, and G. MacDonald, Bispectra of ocean waves, in *Time Series Analysis*, edited by M. Rosenblatt, pp. 125–139, John Wiley, New York, 1963.
Hay, A. E., and A. J. Bowen, Spatially correlated depth changes in the nearshore zone during autumn storms, *J. Geophys. Res.*, *98*, 12,387–12,404, 1993.
Herbers, T. H. C., and M. C. Burton, Nonlinear shoaling of directionally spread waves on a beach, *J. Geophys. Res.*, *102*, 21,101–21,114, 1997.
Herbers, T. H. C., R. L. Lowe, and R. T. Guza, Field observations of orbital velocities and pressure in weakly nonlinear surface gravity waves, *J. Fluid Mech.*, *245*, 413–435, 1992.
Herbers, T. H. C., S. Elgar, and R. T. Guza, Infragravity-frequency (0.005–0.05 Hz) motions on the shelf, part 1, Forced waves, *J. Phys. Oceanogr.*, *24*, 917–927, 1994.
Kraus, N. C., and K. Horikawa, Nearshore sediment transport, in *The Sea*, edited by B. Le Méhauté and D. M. Hanes, vol. 9, part B, pp. 775–813, John Wiley, New York, 1990.
Miche, M., Movements ondulatoires de la mer en profondeur constante ou decroissante, *Ann. Ponts Chaussées*, *114*, 25–406, 1944.
Nielsen, P., *Coastal Bottom Boundary Layers and Sediment Transport*, *Adv. Ser. on Ocean Eng.*, vol. 4, World Sci., River Edge, N. J., 1992.
Norheim, C. A., T. H. C. Herbers, and S. Elgar, Nonlinear evolution of surface wave spectra on a beach, *J. Phys. Oceanogr.*, *28*, 1534–1551, 1998.
Sleath, J. F. A., Sediment transport by waves and currents, *J. Geophys. Res.*, *100*, 10,977–10,986, 1995.
Traykovski, P., A. E. Hay, J. D. Irish, and J. F. Lynch, Geometry, migration, and evolution of wave orbital ripples at LEO-15, *J. Geophys. Res.*, *104*, 1505–1524, 1999.
Vincent, C. E., and P. D. Osborne, Bedform dimensions and migration rates under shoaling and breaking waves, *Cont. Shelf Res.*, *13*, 1267–1280, 1993.
Zedel, L., and A. E. Hay, A coherent Doppler profiler for high-resolution particle velocimetry in the ocean: Laboratory measurements of turbulence and particle flux, *J. Atmos. Oceanic Technol.*, *16*, 1102–1117, 1999.

A. M. Crawford, Mine and Torpedo Defence, Defence R&D Canada-Atlantic, P.O. Box 1012, Dartmouth, Nova Scotia, Canada B2Y 3Z7. (anna.crawford@drdc-rddc. gc.ca)

A. E. Hay, Department of Oceanography, Dalhousie University, Halifax, Nova Scotia, Canada B3H 4J1.